SCIENCE CHINA
Physics, Mechanics & Astronomy

• Article •

September 2013 Vol.56 No.9: 1760–1769
doi: 10.1007/s11433-013-5286-z

Study of nanoscratching of polymers by using molecular dynamics simulations

YUAN DanDan, ZHU PengZhe*, FANG FengZhou & QIU Chen

State Key Laboratory of Precision Measuring Technology and Instruments, Centre of MicroNano Manufacturing Technology, Tianjin University, Tianjin 300072, China

Received April 21, 2013; accepted July 4, 2013; published online July 24, 2013

Molecular dynamic simulations are performed to study the nanoscratching behavior of polymers. The effects of scratching depth, scratching velocity and indenter/polymer interaction strength are investigated. It is found that polymer material in the scratching zone around the indenter can be removed in a ductile manner as the local temperature in the scratching zone exceeds glass transition temperature T_g. The recovery of polymer can be more significant when the temperature approaches or exceeds T_g. The tangential force, normal force and friction coefficient increase as the scratching depth increases. A larger scratching velocity leads to more material deformation and higher pile-up. The tangential force and normal force are larger for a larger scratching velocity whereas the friction coefficient is almost independent of the scratching velocities studied. It is also found that stronger indenter/polymer interaction strength results in a larger tangential force and friction coefficient.

polymer, nanoscratching, molecular dynamics

PACS number(s): 62.25.+g, 81.05.Lg, 62.20.Qp, 31.15.Qg

Citation: Yuan D D, Zhu P Z, Fang F Z, et al. Study of nanoscratching of polymers by using molecular dynamics simulations. Sci China-Phys Mech Astron, 2013, 56: 1760–1769, doi: 10.1007/s11433-013-5286-z

1 Introduction

Polymer materials have a critical role in the fields of nanomanufacturing because of attractive mechanical, optical and electrical properties. In order to fabricate polymer components with high dimensional accuracy and good surface finish, it has become necessary for a better understanding and control of the processing behavior of polymers. Smith [1] employed single point diamond turning to study the machining behavior of polymers and found that the glass transition temperature of the polymers is the most important parameter that governs the surface roughness. Carr and Feger [2] found that the tool speed is an important factor in the materials removal and machined surface roughness. Briscoe et al. [3] investigated the normal and scratch hardness of poly (methylmethacrylate) (PMMA) and found that PMMA presents a far-ranging material response from brittle to ductile and from elastic to plastic during scratching process. Gauthier et al. [4] studied the contact of a moving tip with a polymeric surface and claimed that temperature, strain and strain rate are important factors controlling the type of scratching on polymers. Krupička et al. [5] conducted scratch tests on polymer coatings and found that the scratch speed can affect both the friction and deformation response. Furthermore, Jardret et al. [6] believed that the strain value at fracture depends on the strain rate and temperature, and is independent of the indenter geometry and scratch conditions. Kim et al. [7] investigated the influence of temperature on the tribological properties between PMMA film and fused silica lens. They observed that the friction force increases as the temperature increases and the tribological properties can be altered by the thermal treatment of the PMMA film.

*Corresponding author (email: pengzhezhu@gmail.com)

In addition to experiments, computer simulation techniques such as molecular dynamics (MD) and finite element method (FEM) have also been applied to study the scratching process of polymers. FEM has been used to investigate the effect of constitutive relation on scratch visibility resistance [8], scratch velocity dependence on recovery of viscoelastic-viscoplastic solids [9] and effect of strain hardening and local friction coefficient on the scratch resistance [10]. However, since only a few nanometers or less of the material surface is involved in the nanometric scratching, the material can no longer be considered as a continuum model. Therefore, FEM based on continuum mechanics cannot correctly predict the deformation of material on the nanoscale. Recently, Solar et al. [11] made acomparison between FE and MD simulations for indentation of polymer, which showed that MD simulations are more applicable to investigate the local physics of contact mechanics. MD simulations have been performed to study the formation mechanism of ZnO diatomic chain [12], the bending characteristics of carbon nanotubes (CNT) [13], and the detwinning deformation behavior of nanocrystalline Ni [14]. Furthermore, in the field of nanomachining, MD simulations can also be used to investigate the critical rake angle in nanometric cutting of Cu [15] and friction in nanometric scratching process of Cu [16]. In addition, Solar et al. [17] conducted a scratch test on linear amorphous polymer modeled by a coarse-grained model through MD simulations to study the local friction coefficient. Brostowet al. [18] performed MD simulations of scratching to investigate the tribological behavior of polymers and found that the orientation of the chemical bonds is a major factor affecting the scratch resistance and recovery.

Although some research work has been done to explore the nanoscratching behavior of polymer, a number of important questions remain unsolved, such as how the change of temperature in the scratching zone affects the nanoscratching process of polymers. Therefore, in order to further understand the deformation mechanism of polymers during the nanoscratching process, MD simulations of scratching on the amorphous polymer modeled by a bead-spring model are conducted in this paper. The effects of scratching depth, scratching velocity and the interaction strength between workpiece and indenter on the scratching process will be thoroughly investigated.

2 Molecular model and simulations

2.1 Simulation method

The MD simulation model of nanometric scratching consists of a polymer workpiece and a rigid diamond indenter, as shown in Figure 1. The polymer workpiece is modeled by a classical bead-spring model that represents the coarse-grained behavior of polymers. The non-bonded interactions of beads (monomers) are described by the Lennard-Jones 6–12 potential (eq. (1)) truncated at r_c=2.5σ [19–21]:

$$U(r)=4\varepsilon_{11}\left(\left(\frac{\sigma}{r}\right)^{12}-\left(\frac{\sigma}{r}\right)^{6}\right),\ r\leqslant r_c, \tag{1}$$

where ε_{11}(=2.0ε) is the interaction strength between monomers, and σ is a characteristic length. Bonded beads along a chain are connected by an additional finite extensible nonlinear elastic (FENE) potential (eq. (2)):

$$U_{\text{fene}}(r)=-0.5KR_0^2\ln\left(1-\left(\frac{r}{R_0}\right)^2\right),\ r\leqslant R_0, \tag{2}$$

where K (=30ε/σ^2) is the spring constant, and R_0 (= 1.5σ) is the maximum extent [19–21].

It should be noted that results herein are presented in the dimensionless Lennard-Jones (LJ) units, where time is in units of $\tau=\sigma(m/\varepsilon)^{1/2}$, length is in units of σ, and temperature is in units of ε/k_B (k_B is Boltzmann's constant). Since we aim to study the nanoscratching behavior of PMMA, an approximate conversion for PMMAis presented in Table 1 [22,23] to convert the results into absolute numerical values in SI units.

To generate the amorphous polymer workpiece, 13500 chains with 100 monomers in every chain are randomly placed in a rectangular box. The work piece has a dimension of 188σ, 113σ and 60σ in x, y and z directions, respectively. It is divided into three different regions: Boundary region, Thermostat region and Newtonian region [24], as shown in Figure 1(b). Periodic boundary conditions are used in x and y directions [25]. All simulations are performed with the open source package of Large-scale atomic/molecular massively parallel simulator (LAMMPS) [26].

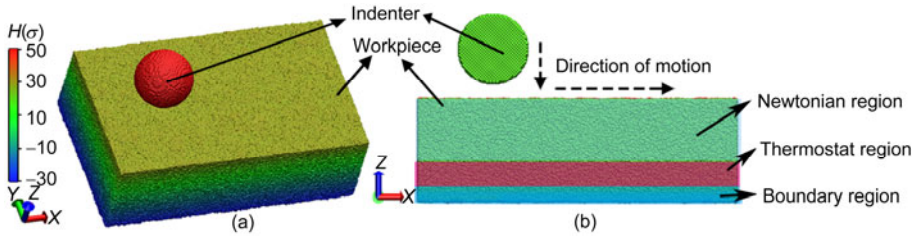

Figure 1 Model of molecular dynamics simulation. (a) Oblique view, (b) section view. Model in (a) is colored according to the height along z direction, and colors in (b) are for separating different regions.

Table 1 Approximate conversion between LJ units and SI units for PMMA ($m = 1.660\times10^{-25}$ kg for each monomer)

Physical quantity	LJ units	Approximate conversion
Time	2.0(τ)	1.9×10^{-12} (s)
Length	1(σ)	0.5×10^{-9} (m)
Energy	1.0(τ)	1.2×10^{-20} (J)
Temperature	0.3–1.0(ε/k_B)	255–850 (K)
Velocity	0.5–2.0(σ/τ)	132–526 (m/s)

Verlet algorithm with a timestep δ_t= 0.01τ is adopted to integrate the Newton's equations of motion. A Langevin thermostat with a damping parameter of 1.0τ is used to prescribe the temperature, and the desired bulk temperature before indenting is set to be 0.3ε/k_B.

The indenter formed by perfect diamond atomic lattice has a spherical shape with radius =20σ. In the simulations the indenter is supposed to be rigid so the interactions between atoms of indenter can be ignored.

The interaction between the polymer monomers and atoms in the indenter is described by Lennard-Jones 6–12 potential with an interaction strength ε_{12}=0.6ε. Various values of ε_{12} are adopted to investigate the effect of interaction strength.

The local temperature distribution of the workpiece is evaluated according to the fundamental relationship between temperature and kinetic energy, see eq. (3) [27] such that

$$T = \frac{\sum_{i=1}^{N} m v_i^2}{3\times N\times k_B}, \tag{3}$$

where k_B is the Boltzmann constant. The workpiece is divided into several cubic cells with the same dimensions of $5\sigma \times 5\sigma \times 5\sigma$. T and N are the average temperature and the number of particles within each cell, respectively. The value of v_i is the velocity for each particle i within each cell. Different sizes of cell (3σ, 5σ, 6σ, 7σ) have been tried to evaluate the influence of cell size on the calculated temperature profile and the general temperature profiles do not show much difference for various cell sizes.

2.2 Simulation procedure

In order to obtain an equilibrium configuration of polymer workpiece, a series of relaxation processes are performed prior to scratching. Initially, the workpiece is equilibrated using microcanonical ensemble (NVE) dynamics with a soft pair potential [20] for 20000 steps. The desired bulk temperature is 0.3ε/k_B. Since the randomly created chains are seriously overlapped, high potential energy is created, which had the possibility to explode. The soft potential under NVE ensemble is used to pushing apart the overlapping particles without adjusting the system volume. The workpiece is relaxed between two repulsive walls concurrently. It can prevent the workpiece from expanding as well as allowing for the existence of the two repulsive walls leading to a flatter workpiece surface for better performing the scratch simulation. The interaction between the wall and the polymer monomer is described by the Lennard-Jones 9–3 potential (see eq. (4)) with interaction strength ε_w = 1.0ε [21] such that

$$U_{\text{wall}}(z) = \varepsilon_w\left(\frac{2}{15}\left(\frac{\sigma}{z}\right)^9 - \left(\frac{\sigma}{z}\right)^3\right), \tag{4}$$

where z is the perpendicular distance between a polymer monomer and the wall. Then the walls are removed and the workpiece is further relaxed with FENE potential and Lennard-Jones potential for another 20000 steps. The workpiece had some degree of shrink during this process as a result of the change of interaction potential. After that the workpiece reaches a somewhat stable state, the indenter is placed above the surface of the polymer workpiece. The bottom is fixed. Then the third relaxation process of 20000 steps is performed. At the end of the relaxation, the bulk temperature fluctuates around the desired value (0.3ε/k_B), and the pressure approaches 0 bar. Afterwards the indenter indents vertically down into the workpiece and then scratches the workpiece horizontally [28]. Snapshots of the indenting scratching process are processed by visual molecular dynamics (VMD) [29]. NVE ensemble is used in both the relaxation process prior to indenting and the scratching process. Since material removal during the nanoscratching process occurs within a few to tens of nanometer range, only a small part of workpiece is involved in this process. The volume of workpiece is nearly unchanged from the macroscopic view. In addition, change of energy has significant influence on the deformation of workpiece, thus it is necessary to study the energy change. Therefore, we use NVE ensemble during the scratching process [30].

2.3 Glass transition temperature of the workpiece

Since glass transition temperature (T_g) is an important parameter that significantly affects the processing property of polymer, the T_g of the workpiece is calculated. The model for calculating the glass transition temperature of the polymer has dimensions of 28.7σ×28.7σ×28.7σ. It is created using the same method as previously described except that periodic boundary conditions are used in the x, y and z directions. The glass transition temperature is evaluated from the change of the slope of the volume–temperature curve [31]. The volume at a certain temperature is obtained by cooling the system from the next higher temperature [32].

The simulations are performed following these steps: First, the system is equilibrated with a soft potential using NVE dynamics at temperature of 1.0ε/k_B to un-overlap the particles. After that the soft potential is replaced with FENE potential and Lennard-Jones potential, followed by relaxa-

tion for 50000 timesteps (δ_t=0.01τ) at temperature of 1.0ε/k_B. Canonical ensemble (NVT) dynamics is used in this stage of relaxation for keeping a constant temperature. Then, the system is equilibrated under 0 bar using the Nose-Hoover method in the isothermal–isobaric (NPT) ensemble for 150000 timesteps. The adoption of NPT ensemble during this stage is to obtain the free volume of polymer changing with temperature. After that the system temperature is cooled down to the desired temperature 0.1ε/k_B for 150000 timesteps followed by further relaxation of 150000 timesteps at the desired temperature [33]. Then the volume of the model under each bulk temperature will be obtained. Since polymers have an abrupt change in volume during the glass transition region, the intersection of the two fitted straight line can give an estimate of the glass transition temperature. As is shown in Figure 2, T_g is approximately 0.76ε/k_B with 100 monomers each chain.

3 Results and discussion

3.1 Nanometric scratching process and recovery

Figure 3 illustrates the typical snapshots during the MD simulation of scratching process. The right side of Figure 3 shows a primary view of the scratching process in half section. Moreover, since the lower part of workpiece has no significant changes during the scratching process, only the upper half of workpiece is demonstrated for improving the display speed of VMD. We have employed a thicker model with a film thickness of 100σ and found that adopting a thicker model does not change the conclusions obtained from the model in Figure 1. In the simulation, the initial bulk temperature of workpiece is 0.3ε/k_B, which is below T_g. The scratching velocity is 1.0σ/τ, the scratching depth is 10σ and ε_{12}=0.6ε. It is important to note that the discussions for the results demonstrated here are not just based on the typical snapshots, but also on the observation of the dynamic process of scratching. As can be seen in Figure 3, with the increase of scratching distance, chip forms as some workpiece particles pile up in front of the indenter. A groove is fabricated after scratching.

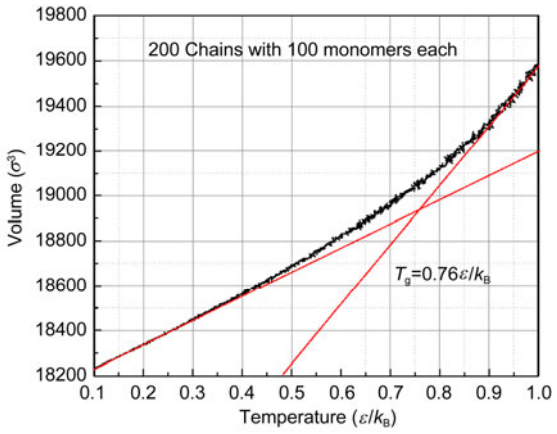

Figure 2 Volume–temperature cooling curves which is used for determining the glass transition temperature.

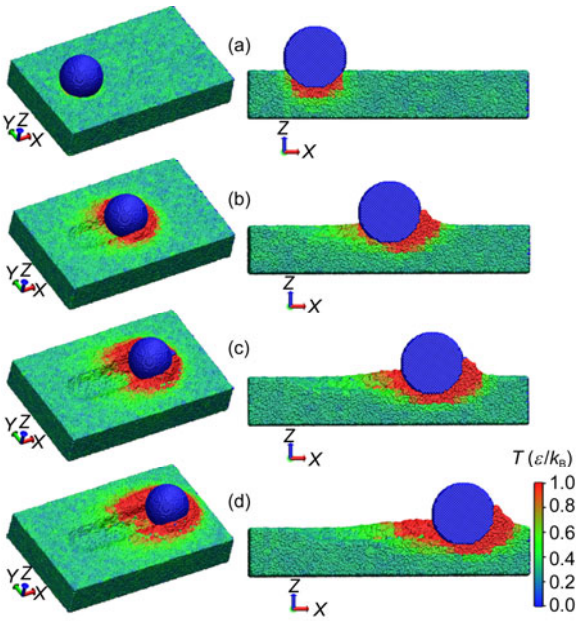

Figure 3 Typical snapshots of workpiece obtained during the scratching process. (a) indenting down to depth of 10σ, (b)–(d) scratching distance of (b) 50σ, (c) 75σ and (d) 100σ. The workpiece is colored according to the temperature distribution. Only the upper half of workpiece is demonstrated for improving the display speed.

In order to improve the visibility of the temperature distribution of workpiece, the color bar scales for local temperature distribution in this paper are all set to be 0.0ε/k_B –1.0ε/k_B. However it should be noted that the range of the color bar does not correspond to the actual range of local temperature. From Figure 3, it can be seen clearly that the local temperature of scratching zone is higher than T_g. This indicates that the workpiece in the scratching zone can be removed in a ductile manner as claimed by Smith [1] in the study of single point diamond turning process of polymers. Moreover, with the advance of indenter, more materials are deformed plastically. More heat is generated and dissipated into the polymer, thus lead to the local temperature of scratching zone exceeding T_g. After scratching for a certain distance, the energy exchange reaches an steady state.

Tangential force and normal force are two important parameters to investigate the nanometric machining process. In this paper, tangential force and normal force are super summation of the atomic forces of workpiece on the indenter. The force–distance curves are presented in Figure 4. During the indenting process, the normal force increases rapidly and the tangential force remains nearly zero. After indentation, when the indenter is sliding along the scratch direction, the normal force abruptly declines and the tangential force increases at the beginning of scratching. This is because the indenter-workpiece contact projection area in

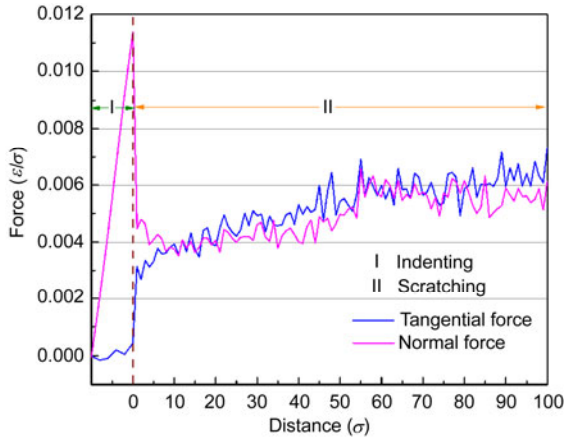

Figure 4 Force–distance curves during the indenting and scratching process.

the normal direction decreases at the initial stage of scratch while the situation in the scratching direction is the opposite. Both the normal force and tangential force tend to be steady and only fluctuate around the average values after scratching for 55σ, which indicates the scratching reaches a steady state.

Because of the viscoelasticity of polymers, the polymers will recover a portion of their initial deformation after deformed by an external force [34]. In order to observe the elastic recovery, the indenter is removed after scratching, and then the polymer workpiece is relaxed for a certain amount of timesteps [35]. Simulations are performed under various temperatures to study the temperature dependence on elastic recovery. The obtained results are shown in Figure 5. It should be noted that the particles with height below the scratching depth are removed in Figure 5 for better observations. The color bar scales for height are set to be -30σ–50σ for a better presentation. However, the range of the color bar does not correspond to the actual range of the pile-up height of model.

From Figure 5, it can be seen that some materials still exist in the groove after scratching. The pile-ups have different degrees of collapse at various temperatures because of the sudden remove of indenter. At temperature of $0.3\varepsilon/k_B$, which is far below the glass transition temperature T_g, the groove morphology does not show much change with the relaxed time increases (see Figure 5(a)). At the temperature of $0.7\varepsilon/k_B$ and $1.0\varepsilon/k_B$, which are close to T_g and above T_g respectively, both the traces of grooves become fuzzy after the relaxation. Moreover, the recovery is more obvious with the increase of temperature. This indicates that temperature has a significant influence on the recovery of polymer deformation. When the temperature approaches T_g or above T_g, the viscoelasticity of polymer can be more obvious.

3.2 Influence of scratching depth

In order to investigate the effects of scratching depth simulations are carried out at three different scratching depths (5σ, 10σ, and 15σ). The scratching velocity is $1.0\sigma/\tau$, the initial bulk temperature is $0.3\varepsilon/k_B$, and $\varepsilon_{12} = 0.6\varepsilon$.

Figures 6(a)–(c) presents the final configurations at various scratching depths. The color bar scales for height set to be -30σ–50σ is for a better presentation and comparison of the pile-up heights, rather than the actual range of the pile-up height of model. It can be seen that at a small scratching depth the workpiece material is only displaced around the indenter and there is no indication of chip formation in this region, which indicates the dominate wear mechanism is ploughing, as shown in Figure 6(a). Whereas at a bigger scratching depth, the workpiece material is detached from the workpiece in the form of chips, which

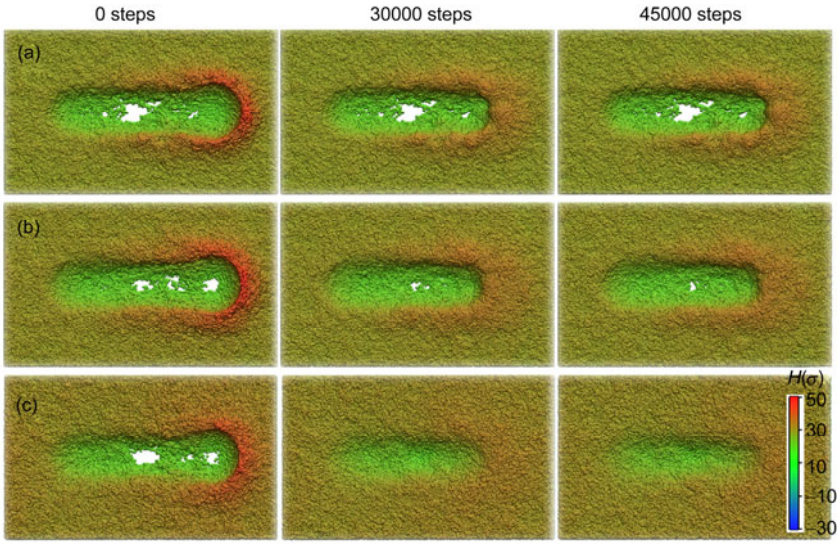

Figure 5 Recovery over time at various temperatures: (a) $0.3\varepsilon/k_B$; (b) $0.7\varepsilon/k_B$; (c) $1.0\varepsilon/k_B$. The workpieces are displayed in top view and colored according to the height along z direction. The particles with height below the scratching depth are removed for better observations.

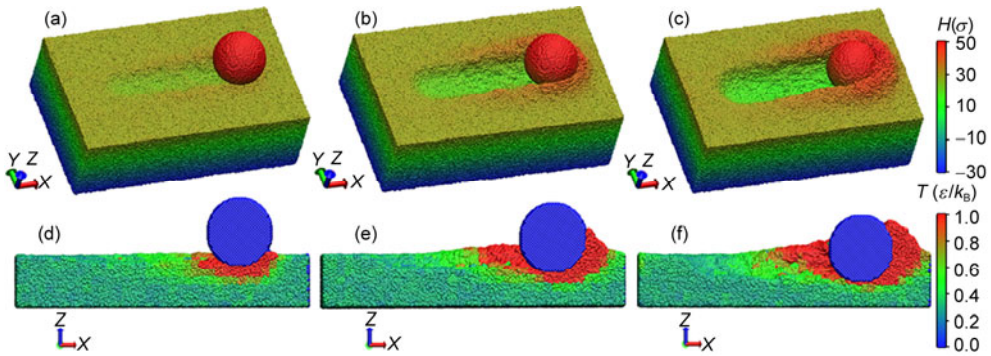

Figure 6 Final configurations and temperature distributions at various scratching depths of: (a)&(d) 5σ, (b)&(e) 10σ and (c)&(f) 15σ. The workpiece in (a)–(c) is colored according to the height along z direction. The workpiece in (d)–(f) is colored according to the temperature, and only the upper half of workpiece is demonstrated for improving the display speed.

indicates the wear is dominated by cutting, see Figures 6(b) and (c). In order to give a quantitative comparison of the pile-ups in front of the indenter at different scratching depths, the pile-up heights are calculated. In this study pile-up heights are determined by the difference between the height of the highest particle in the pile-up and the height of the initial upper surface of workpiece. As can be seen in Figure 7, the pile-up heights increase significantly as the scratching depth increases.

Figures 6(d)–(f) illustrates the temperature distributions of the workpiece at various scratching depths. The color bar scales in Figures 6(d)–(f) are all set to be $0.0\varepsilon/k_{\mathrm{B}}$–$1.0\varepsilon/k_{\mathrm{B}}$. This scale can give an explicit display of the temperature distribution of workpiece as mentioned earlier. And for the purpose of comparison, the upper limits of the color bars all set the same value at different scratching conditions. It can be seen that the high temperature zone with temperature over T_{g} becomes larger as the scratching depth increases. This is because atagreater scratching depth the indenter contacts more polymer chains and more mechanical energy is converted to thermal energy (heat).

Figure 8(a) shows the average forces at various scratching depths. The average forces are calculated for the scratching distance from 10σ to 100σ where the forces have no abrupt changes. The friction coefficient is also obtained from the ratio of the average tangential force to the average normal force for a measurement of the scratching resistance, as shown in Figure 8(b). From Figure 8(a), it can be seen that a greater scratching depth leads to bigger tangential force and normal force. This is because at a greater scratching depth the indenter contacts more workpiece material,

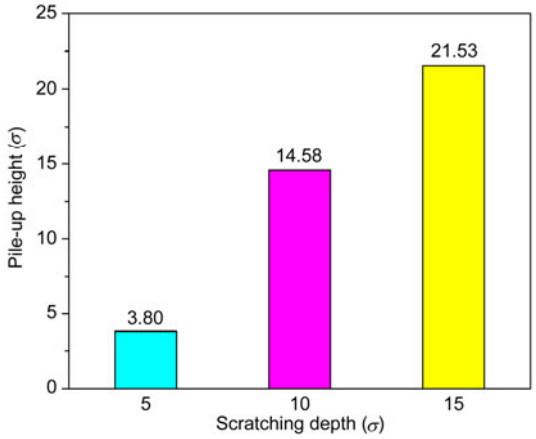

Figure 7 Pile-up heights at various scratching depths.

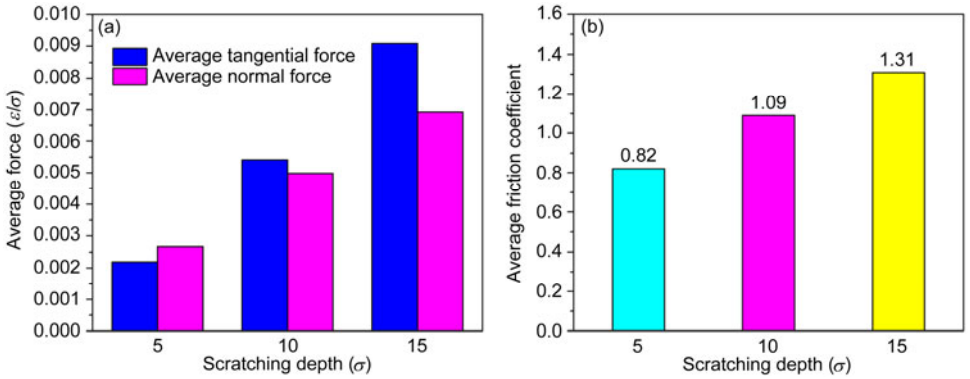

Figure 8 (a) Average forces and (b) average friction coefficients at various scratching depths.

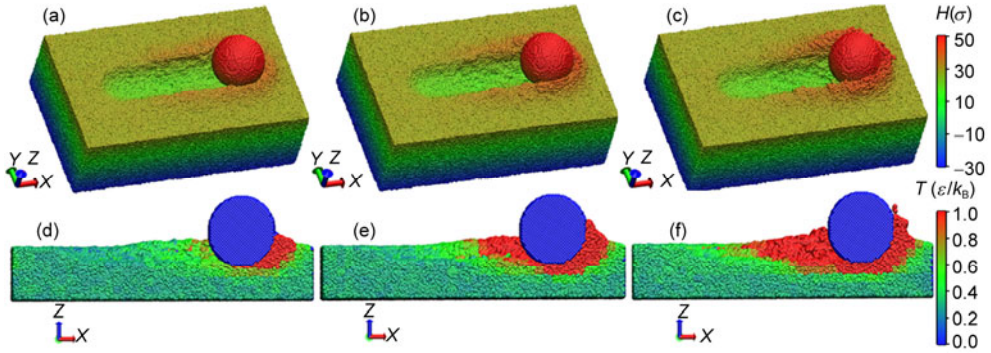

Figure 9 Final configurations and temperature distributions at various scratching velocities of: (a)&(d) $0.5\sigma/\tau$, (b)&(e) $1.0\sigma/\tau$ and (c)&(f) $2.0\sigma/\tau$. The workpiece in (a)–(c) is colored according to the height along z direction. The workpiece in (d)–(f) is colored according to the temperature, and only the upper half of workpiece is demonstrated for improving the display speed.

thus resulting in bigger forces. In addition, although both tangential force and normal increase with the scratching depth increases, the tangential force increases more rapidly than the normal force since more material deformation exists and more pile-up forms in front of the indenter. Consequently, the friction coefficient increases from below to above the value of 1.0 with the increase of scratching depth from 5σ to 15σ.

3.3 Influence of scratching velocity

MD simulations are performed at various velocities ($0.5\sigma/\tau$, $1.0\sigma/\tau$, and $2.0\sigma/\tau$) for exploring the effect of scratching velocity on the scratching process. The scratching depth is 10σ, the initial bulk temperature is $0.3\varepsilon/k_{\mathrm{B}}$ and ε_{12} is 0.6ε.

Figures 9(a)–(c) present the final configurations at various scratching velocities and the corresponding temperature distributions of the workpiece are shown in Figures 9(d)–(f). As can be seen from Figures 9(a)–(c) and Figure 10, the pile-ups in front of the indenter increase significantly with the increase of scratching velocity. The larger pile-up height at a larger scratching velocity indicates more resistance to motion in the scratching process, which leads to a greater tangential force. Moreover, the deformation rate will become too high for the polymers to respond at higher scratching velocities [2]. The material will bring a higher resistance to the plastic deformation, known as the strain rate hardening effect [36], which can lead to the increase of tangential force and normal force. However, there is only a slight increase of the tangential force compared with the significant increase of pile-up height, as shown in Figure 11(a). In fact, with the increase of scratching velocity, there is less time available for the heat energy to dissipate into the bulk of the polymer [36]. The increasing scratching velocity generates a larger amount of heat per unit time, which leads to a higher temperature in the scratching zone. As can be seen from Figures 9(d)–(f), the high temperature zone with temperature exceeds T_{g} becomes larger with the increase of

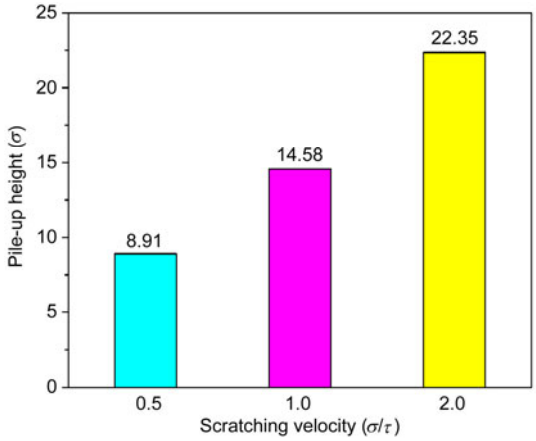

Figure 10 Pile-up heights at various scratching velocities.

scratching velocity. The heat generated can increase the long-range mobility of the polymer chains, thus leading to the reduction of tensile strength and shear stress, as shown by Xiao et al. [37]. The thermal softness effect allows the workpiece to be machined more easily, reducing the tangential force and normal force. Based on the time- temperature super position principle [38,39], the increase in deformation rate can compensate for the loss of material strength caused by the temperature rise in the scratching zone. This implies that the effects of pile-up, heat and strain rate hardening on the scratching forces compete during the scratching process. The increase of the forces with the increase of scratching velocity indicates that the pile-up and strain rate hardening effect plays a more significant part in determining scratching forces.

Figure 11(b) shows the average friction coefficients at various scratching velocities. As the scratching velocity increases, the tangential force and the normal force also increase. Because of the combination of the three main factors: pile-up, thermal softness and strain rate hardening effect, the friction coefficients are nearly constant at different scratching velocities. This indicates that the friction coefficient is independent of the scratching velocity studied.

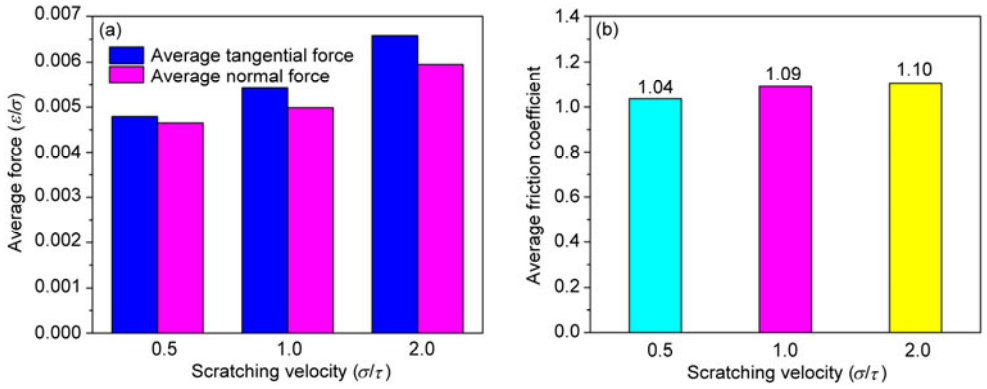

Figure 11 (a) Average forces and (b) average friction coefficients at various scratching velocities.

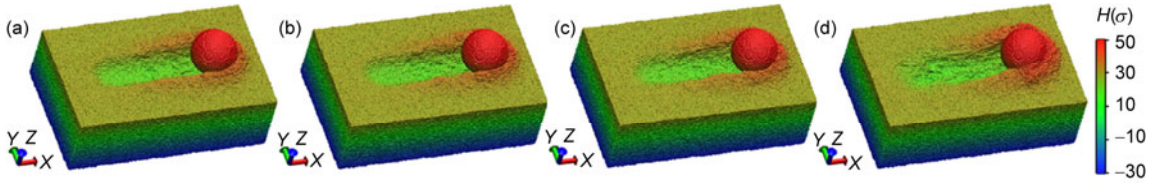

Figure 12 Final configurations at various values of ε_{12} of: (a) 0.3ε, (b) 0.6ε, (c) 1.0ε and (d) 4.0ε.

3.4 Influence of the interaction strength between the indenter and workpiece

To study the effect of polymer/indenter interaction ε_{12}, different values of ε_{12} (0.3ε, 0.6ε, 1.0ε and 4.0ε) are adopted in the simulations. In the simulations the scratching depth is 10σ, the initial bulk temperature is $0.3\varepsilon/k_B$, and scratching velocity is $1.0\sigma/\tau$.

Figure 12 shows the final configurations of simulated model at various values of ε_{12} in the scratching process. The pile-up heights at various values of ε_{12} are shown in Figure 13. It can be seen that as the indenter/polymer interaction becomes stronger, more pile-up is formed around the indenter. This can be noted that when the indenter/polymer interaction is stronger, more workpiece material is extruded.

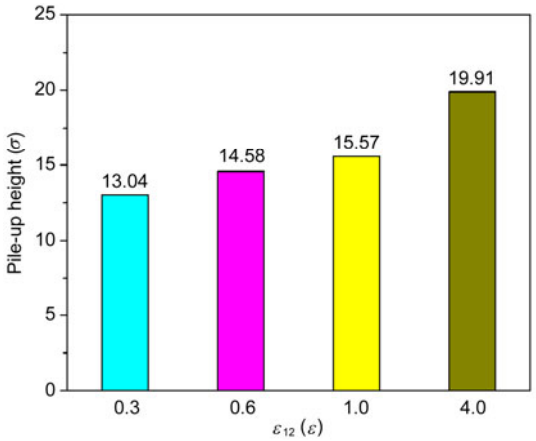

Figure 13 Pile-up heights at various values of ε_{12}.

Figures 14(a) and (b) show the average forces and friction coefficients, respectively. The average tangential force is bigger for a larger indenter/polymer interaction. However, the normal force does not exhibit much changes as the ε_{12} varies. Therefore, the friction coefficient increases as the indenter/polymer interaction increases.

4 Conclusions

In this paper a series of molecular dynamics simulations are performed to investigate the nanoscratching process of bead- spring polymers using rigid indenter. The glass transition temperature of the polymer is caculated in order to better understand the scratching behavor of the polymer. The simulations are performed to investigate the effects of scratching depth, scratching velocity and the interaction strength between polymer and indenter on the deformation behavior of polymer. The obtained results can be summarized as follows:

Firstly, during the scratching process, the local temperature in the scratching zone is higher than T_g, which indicates that the workpiece in the scratching zone can be removed in a ductile manner. The temperature has a significant influence on the recovery of polymer deformation. When the temperature approaches T_g or above T_g, the recovery of polymer can be more obvious.

Secondly, a greater scratching depth results in more material deformation and larger pile-up height. As a result, the indenter meets more resistance during the scratching, thus leading to larger tangential force and normal force. The friction coefficient also increases as the scratching depth

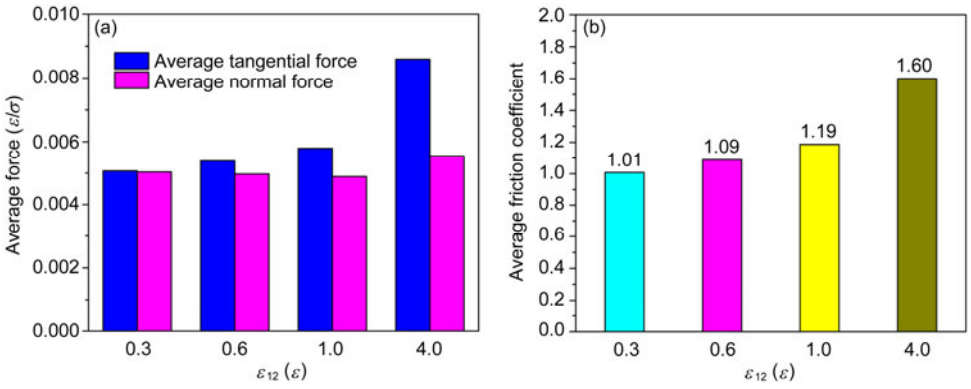

Figure 14 (Color online) (a) Average forces and (b) average friction coefficients at various values of ε_{12}.

increases. Moreover, as more polymer chains are displaced by the indenter, more heat is generated in the contact zone.

Thirdly, the scratching velocity mainly exerts three different influences on the machining behavior of polymer workpiece. The first is that the pile-ups in front of the indenter increase significantly with the increase of scratching velocity. This can bring more resistance to the indenter. Second, a higher velocity leads to a higher deformation rate and the strain rate hardening effect prevails, which can also lead to a greater tangential force and normal force. Finally, at a higher scratching velocity more heat is generated in the scratching zone, the long-range mobility of the polymer chains increases, resulting in the reduction of tensile strength and shear stress. The workpiece can be machined more easily due to the thermal softness effect. Owing to combined effects of the three factors, the friction coefficients are nearly constant for different scratching velocities studied.

Lastly, a stronger indenter/polymer interaction strength results in a larger pile-up height, thus leading to a bigger tangential force. The friction coefficient shows similar trends. Whereas the normal force exhibits no significant changes as the indenter/polymer interaction strength increases.

This work was supported by the National Natural Science Foundation of China (Grant No. 90923038), the National Basic Research Program of China (Grant No. 2011CB706703) and "111" project (Grant No. B07014) by the State Administration of Foreign Experts Affairs and the Ministry of Education of China.

1 Smith E F. Single-point Diamond Turning of Amorphous Thermoplastic Polymers. Dissertation for the Master Degree. Raleigh: North Carolina State University, 1989
2 Carr J W, Feger C. Ultraprecision machining of polymers. Precis Eng, 1993, 15: 221–237
3 Briscoe B J, Evans P D, Biswas S K, et al. The hardnesses of poly (methylmethacrylate). Tribol Int, 1996, 29: 93–104
4 Gauthier C, Lafaye S, Schirrer R. Elastic recovery of a scratch in a polymeric surface: experiments and analysis. Tribol Int, 2001, 34: 469–479
5 Krupička A, Johansson M, Hult A. Use and interpretation of scratch tests on ductile polymer coatings. Prog Org Coat, 2003, 46: 32–48
6 Jardret V, Morel P. Viscoelastic effects on the scratch resistance of polymers: relationship between mechanical properties and scratch properties at various temperatures. Prog Org Coat, 2003, 48: 322–331
7 Kim K S, Heo J C, Kim K W. Effects of thermal treatment on the tribologicalcharacteristics of thermoplastic polymer film. Thin Solid Films, 2011, 519: 5988–5995
8 Hossain M M, Jiang H, Sue H J. Effect of constitutive behavior on scratch visibility resistance of polymers–A finite element method parametric study. Wear, 2011, 270: 751–759
9 Aleksy N, Kermouche G, Vautrin A, et al. Numerical study of scratch velocity effect on recovery of viscoelastic-viscoplastic solids. Int J Mech Sci, 2010, 52: 455–463
10 Pelletier H, Krier J, Gauthier C. Influence of local friction coefficient and strain hardening on the scratch resistance of polymeric surfaces investigated by finite element modeling. Procedia Eng, 2011, 10: 1772–1778
11 Solar M, Meyer H, Gauthier C, et al. Mechanical behavior of linear amorphous polymers: Comparison between molecular dynamics and finite-element simulations. Phys Rev E, 2012, 85: 021808
12 Wang B B, Wang F C, Zhao Y P. Understanding formation mechanism of ZnO diatomic chain and multi-shell structure using physical mechanics: Molecular dynamics and first-principle simulations. Sci China-Phys Mech Astron, 2012, 55: 1138–1146
13 Liang Y J, Han Q. Prediction of nonlocal scale parameter for carbon nanotubes. Sci China-Phys Mech Astron, 2012, 55: 1670–1678
14 Su H, Tang Q H. MD simulations of loading rate dependence of detwinning deformation in nanocrystalline Ni. Sci China-PhysMech Astron, 2013, 56: 491–497
15 Lai M, ZhangX D, Fang F Z. Study on critical rake angle in nanometric cutting. Appl Phys A, 2012, 108: 809–818
16 Zhu P Z, Hu Y Z, Ma T B, et al. Molecular dynamics study on friction due to ploughing and adhesion in nanometric scratching process. Tribol Lett, 2011, 41: 41–46
17 Solar M, Meyer H, Gauthier C, et al. Molecular dynamics simulations of the scratch test on linear amorphous polymer surfaces: A study of the local friction coefficient. Wear, 2011, 271: 2751–2758
18 Brostow W, Hinze J A, Simões R. Tribological behavior of polymers simulated by molecular dynamics. J Mater Res, 2004, 19: 851–856
19 Kremer K, Grest G S. Dynamics of entangled linear polymer melts: A molecular-dynamics simulation. J Chem Phys, 1990, 92: 5057–5086
20 Auhl R, Everaers R, Grest G S, et al. Equilibration of long chain polymer melts in computer simulations. J Chem Phys, 2003, 119: 12718–12728

21 Chandross M, Grest G S. Molecular scale modeling of polymer imprint nanolithography. Langmuir, 2012, 28: 1049–1055
22 Solar M, Meyer H, Gauthier C, et al. Molecular dynamics simulations as a way to investigate the local physics of contact mechanics: a comparison between experimental data and numerical results. J Phys D-Appl Phys, 2010, 43: 455406
23 Solar M, Meyer H, Gauthier C. Analysis of local properties during a scratch test on a polymeric surface using molecular dynamics simulations. Eur Phys J E, 2013, 36: 29
24 Zhu P Z, Hu Y Z, Ma T B, et al. Study of AFM-based nanometric cutting process using molecular dynamics. Appl Surf Sci, 2010, 256: 7160–7165
25 Zhu P Z, Fang F Z. Molecular dynamics simulations of nanoindentation of monocrystalline germanium. Appl Phys A, 2012, 108: 415–421
26 Plimpton S J. Fast parallel algorithms for short-range molecular dynamics. J Comput Phys, 1995, 117: 1–19
27 Ercolessi F. A molecular dynamics primer. In: Spring college in computational physics, ICTP, Trieste, 1997
28 Zhu P Z, Hu Y Z, Wang H, et al. Study of effect of indenter shape in nanometric scratching process using molecular dynamics. Mat Sci Eng A, 2011, 528: 4522–4527
29 Humphrey W, Dalke A, Schulten K. VMD–visual molecular dynamics. J Mol Graph, 1996, 14: 33–38
30 Zhang J J. Molecular Dynamics Study of Generation Mechanism of Surface Layer in Nanomechanical Machining of Crystalline Copper. Dissertation for the Doctoral Degree. Harbin: Harbin Institute of Technology, 2011
31 Rigby D, Roe R J. Molecular dynamics simulation of polymer liquid and glass. I. Glass transition. J ChemPhys, 1987, 87: 7285–7292
32 Han J, Gee R H, Boyd R H. Glass transition temperatures of polymers from molecular dynamics simulations. Macromolecules, 1994, 27: 7781–7784
33 Hossain D, Tschopp M A, Ward D K, et al. Molecular dynamics simulations of deformation mechanisms of amorphous polyethylene. Polymer, 2010, 51: 6071–6083
34 Hilbig T. Scratch Modeling of Polymeric Materials with Molecular Dynamics. Dissertation for the Master Degree. Denton: University of North Texas, 2012
35 Yang Z Y, Jiao F F, Lu Z X, et al. Coupling effects of stress and ion irradiation on the mechanical behaviors of copper nanowires. Sci China-Phys Mech Astron, 2013, 56: 498–505
36 Briscoe B J, Pelillo E, Sinha S K. Scratch hardness and deformation maps for PC and PE. Polym Eng Sci, 1996, 36: 2996–3005
37 Xiao K Q, Zhang L C. The role of viscous deformation in the machining of polymers. Int J Mech Sci, 2002, 44: 2317–2336
38 Andrews R D, Tobolsky A V. Elastoviscousproperties of polyisobutylene. IV. Relaxation time spectrum and calculation of bulk viscosity. J Polym Sci, 1952, 7: 221–242
39 Li R Z. Time-temperature superposition method for glass transition temperature of plastic materials. Mat Sci Eng A, 2000, 278: 36–45